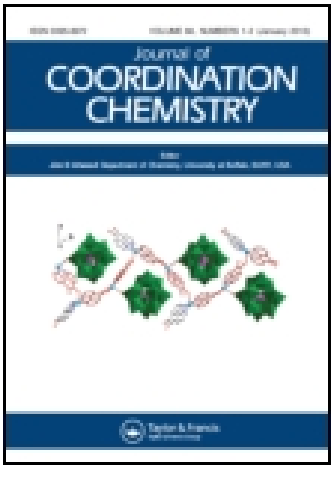

Journal of Coordination Chemistry
Publication details, including instructions for authors and subscription information:
http://www.tandfonline.com/loi/gcoo20

Ultrasound and solvent-induced reversible chromism in a luminescent chalcogenidostannate

Hai-Yun Ren[a], Zhi-Xue Ning[a] & Juan-Juan Hou[a]
[a] School of Chemistry & Material Science, Shanxi Normal University, Linfen, PR China
Accepted author version posted online: 06 Mar 2014.Published online: 28 Mar 2014.

To cite this article: Hai-Yun Ren, Zhi-Xue Ning & Juan-Juan Hou (2014) Ultrasound and solvent-induced reversible chromism in a luminescent chalcogenidostannate, Journal of Coordination Chemistry, 67:6, 1079-1087, DOI: 10.1080/00958972.2014.901505

To link to this article: http://dx.doi.org/10.1080/00958972.2014.901505

Journal of Coordination Chemistry, 2014
Vol. 67, No. 6, 1079–1087, http://dx.doi.org/10.1080/00958972.2014.901505

Ultrasound and solvent-induced reversible chromism in a luminescent chalcogenidostannate

HAI-YUN REN*, ZHI-XUE NING and JUAN-JUAN HOU

School of Chemistry & Material Science, Shanxi Normal University, Linfen, PR China

(*Received 7 September 2013; accepted 1 February 2014*)

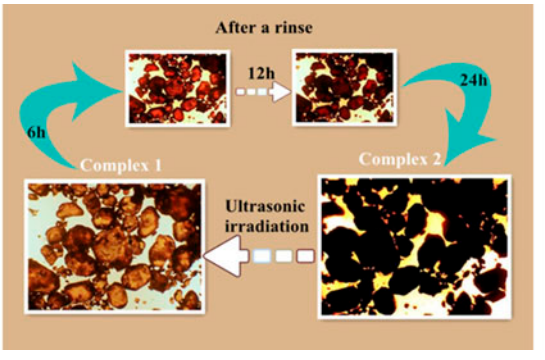

Solvothermal treatment of a mixture of Se, $SnC1_2$, $CoC1_2$, and dien (dien = diethylenetriamine) generated yellow crystals of $[Co(dien)_2]_2Sn_2Se_6$ (**1**), which could transform into black **2** with the same formula via rinsing with water. In the presence of water, ultrasound irradiation of black **2** went back to yellow **1**. The reversible ultrasound and solvent-induced chromism has never been observed before. Compared with yellow **1**, hyperchromism was apparent around 550 nm in the visible absorption spectrum of **2**. The fluorescent properties for **1** and **2** were investigated and the mechanisms were validated by density functional theory calculations on the experimental geometries. In addition, electron paramagnetic resonance spectra of yellow **1** are similar to chromic black **2** in the signal at $g = 4.22$ and $g = 2.19$; the signal at $g = 2.19$ of **2** shows a sharp increase.

Keywords: Ultrasound; Chromism; Chalcogenide; Luminescence

1. Introduction

Chromism attracts attention due to applications in advertisement gadgets, pressure sensors, nonlinear optical devices, molecular devices and possibly most importantly, security features [1]. When given stimulus, such as light, solvent, temperature, and pH, materials may exhibit photochromism, solvatochromism, thermochromism, electrochromism, mechanochromism, vapor-chromism, etc. [2–11]. Chromism may occur when, among solid

*Corresponding author. Email: renhy@sxnu.edu.cn

compounds, changes of the geometrical or electronical structure take place, which affect the physicochemical properties [12]. Thus, one strategy for fabricating chromic compounds is to change their geometrical or electronic structures by embedding a functional group (such as chromophore) into a variety of polymeric matrices. The combination of chromism with additional functionality should lead to multimodally stimuli-responsive systems that would be applied to more sophisticated and broader fields.

The surfactant templating route has recently been extended to new chalcogenidostannates ($[Sn_xQ_y]^{n-}$, Q = S, Se, and Te). In 1996, Kanatzidis first used chelating ethylenediamine as template to synthesize chalcogenidostannates [13]. Chelating amines not only act as solvent but also catalyze chalcogenide Q to gain electrons to form Q^{2-} during the reaction. Chelating amines can also coordinate metal ions to form complex cations as charge compensators. Among chelating amines, diethylenetriamine (dien) may be a tridentate or bidentate nitrogen donor to metal ions.

In contrast to nickel, iron, and manganese, divalent cobalt allows for a larger variety of coordination polyhedra, such as octahedral, tetrahedral, square-pyramidal, trigonal-bipyramidal, and square-planar, and cobalt-containing compounds can have a wide range of colors. Cobalt also shows rich electronic structures. For example, octahedral coordinated Co (II) has high-spin and low-spin electronic configurations that may transit mutually under certain circumstances. These advantages make Co(II) suitable to study chromism. We demonstrate herein a cobalt chalcogenidostannate, $[Co(dien)_2]_2[Sn_2Se_6]$ (**1**), which is constructed by $[Co(dien)_2]^{2+}$ and $[Sn_2Se_6]^{4-}$, which exhibits reversible chromism. After rinsing with water, **1** can transform from yellow to black **2** that can reversibly go back to **1** upon irradiation with ultrasound. This interesting ultrasonic chromism has not previously been reported. The visible solid absorption spectra indicated that the chromism might be a clue to van der Waals interaction between two excited chromophores in the 3-D supramolecular ordered structure.

2. Experimental

2.1. *Materials and physical measurements*

The starting materials were commercially reagent grade and used without purification. FT-IR spectra were recorded from KBr pellets at 400–4000 cm^{-1} on a Nicolet 5DX spectrometer. Elemental analyses were performed on a Perkin-Elmer 240 elemental analyzer. Thermal analyses were carried out in air using SETARAM LABSYS equipment with a heating rate of 10 °C min^{-1}, both of which in air are stable to 270 °C (figure S2). UV–Vis absorption spectra were recorded on a Cary 5000 (VARIAN) UV–Vis–NIR spectrophotometer in a cell with 1 mm width. Photoluminescence was performed on an Edinburgh FLS920 luminescence spectrometer. Electron paramagnetic resonance (EPR) spectra were recorded with a Bruker A300-10/12 EPR spectrometer.

2.2. *Syntheses $[Co(dien)_2]_2[Sn_2Se_6]$ (1)*

Solvothermal treatment of a mixture of Se (0.039 g, 0.5 mM), $SnC1_2{\cdot}2H_2O$ (0.047 g, 0.2 mM), $CoC1_2{\cdot}6H_2O$ (0.049 g, 0.2 mM), and dien (2.5 mL) in a molar ratio of 5 : 2 : 2 : 232 at 160 °C in a Teflon-lined stainless autoclave for 7 days afforded **1** as yellow

brick crystals. Yield 93%. Anal. Calcd for $[Co(dien)_2]_2Sn_2Se_6$: C, 15.23; H, 4.28; N, 13.45. Found: C, 15.46; H, 4.19; N, 13.53. IR (KBr, cm^{-1}): 3237m, 3133m, 2967w, 1621m, 1574m, 1470s, 1385m, 1323m, 1281m, 1238m, 1181m, 1080 *versus* 1042m, 995m, 961 *versus* 860m, 783m, 675m, 633m, 598m.

2.3. *X-ray crystallography*

Data were collected at 298 K on a Bruker Apex diffractometer (Mo-Kα, $\lambda = 0.71073$ Å). Lorentz-polarization and absorption corrections were applied. The structure was solved with direct methods and refined with full-matrix least-squares (SHELX-97) [14]. Analytical expressions of neutral-atom scattering factors were employed and anomalous dispersion corrections were incorporated. All non-hydrogen atoms were refined anisotropically. The crystallographic data are listed in table 1. Selected bond lengths and angles for **1** and **2** are given in table S1 (see online supplemental material at http://dx.doi.org/10.1080/00958972.2014.901505). Distances and angles of the hydrogen bond interactions in **1** and **2** are given in tables S2 and S3, respectively (Supplementary material).

3. Results and discussion

3.1. *Description of structures*

Single-crystal X-ray diffraction analyses reveal that **1** and **2** are isostructural. Thus, only **1** is discussed in detail. Compound **1** crystallizes in the monoclinic space group $P2_1/n$. The asymmetric unit contains one crystallographically independent Co(II), two dien ligands, one

Table 1. Crystal data and structure refinement for **1** and **2**.

	1	**2**
Formula	$C_8H_{26}CoN_6Se_3Sn$	$C_8H_{26}CoN_6Se_3Sn$
Fw	620.85	620.85
Crystal system	Monoclinic	Monoclinic
Space group	$P2_1/n$	$P2_1/n$
a (Å)	10.2224(4)	10.1966(3)
b (Å)	14.5788(6)	14.5846(5)
c (Å)	12.3921(5)	12.3765(4)
β (°)	91.2370(10)	91.2980(10)
V (Å^3)	1846.37(13)	1840.08(10)
Z	4	4
ρ_{Calcd} (g cm^{-3})	2.233	2.241
μ (mm^{-1})	8.162	8.190
$F(0\,0\,0)$	1180	1180
Size (mm)	0.24 × 0.18 × 0.18	0.18 × 0.16 × 0.12
Reflections	11,257/4332	10,267/4398
T_{max}/T_{min}	0.3213/0.2448	0.4398/0.3203
Data/parameters	4332/172	4398/172
S	0.963	1.272
R_1[a]	0.0359	0.0323
wR_2[b]	0.0863	0.0914
$\Delta\rho_{max}/\Delta\rho_{min}$ (e A^{-3})	0.737/−0.921	1.151/−1.032

[a] $R_1 = \sum||F_o| - |F_c||/\sum|F_o|$.
[b] $wR_2 = [\sum w(F_o^2 - F_c^2)^2/\sum w(F_o^2)^2]^{1/2}$.

Sn(IV), and three Se. The Co(II) has slightly distorted octahedral geometry coordinated by six nitrogens from the two trichelating diens (Co1–N1, 2.169(3); Co1–N2, 2.153(3); Co1–N3, 2.174(3); Co1–N4, 2.167(3); Co1–N5, 2.136(3); Co1–N6, 2.200(3) Å). The *cis*-N–Co–N and *trans*-N–Co–N bond angles change from 80.28(13)° to 100.58(13)°, and from 177.35(13)° to 179.07(13)°, respectively. Co(II) with the two tridentate diens forms an octahedral $[Co(dien)_2]^{2+}$, whose conformation is *s*-facial [15, 16]. It is isostructural with cations observed in $[Co(dien)_2]_3[As_3S_6]_2$, $[Co(dien)_2]HgSb_2S_5$, $[Co(dien)_2]As_2Se_6$, and $[Co(dien)_2]_2GeSb_4S_{10}$ [17–25]. Compared with these cations, the $[Co(dien)_2]^{2+}$ of **1** is much less distorted. Sn(IV) shows distorted tetrahedral coordination geometry, consisting of Se1, Se2, Se3, and Se3A from two terminal Se and two μ_2-Se ions. The two $SnSe_4$ tetrahedra are bridged by two μ_2-Se to form a dimeric anionic $[Sn_2Se_6]^{4-}$, in which there are terminal and bridging Sn–Se bonds. The terminal Sn–Se distances are 2.456–2.473 Å and the bridging Sn–Se lengths range from 2.577 to 2.579 Å. It is obvious that the terminal Sn–Se bond is slightly shorter than the bridged ones, consistent with those found in other chalcogenidostannates [26–32]. The Se–Sn–Se bond angles change from 85.755(14)° to 113.680(17)°, which deviates from 109.5° of a perfect tetrahedron. The Se3–Sn1–Se3A bond angle is 94.245(14)° and the Sn1A–Se3–Sn1 bond angle is 85.755(14)°. The two Sn(IV) ions and two μ_2-Se atoms form a coplanar four-membered ring of $\{Sn_2Se_2\}$ [figure 1(a)], similar to $[Sn_2S_6]^{4-}$ reported by Dai *et al.* [15, 16].

Adjacent $[Co(dien)_2]^{2+}$ dications and dimeric anionic $[Sn_2Se_6]^{4-}$ are packed via weak N-H···Se hydrogen bonds to form the final 3-D supramolecular framework [figure 1(b)]. The H···Se bond lengths fall in the range of 2.62–2.93 Å and N–H···Se angles range from 145° to 173°, respectively (table S2 of the Supplementary material). The H···Se lengths and N–H···Se angles are consistent with values in the literature [33–35].

In contrast to the structure of **1**, Co(II) of **2** shows squeezed octahedral geometry, in which the equatorial Co1–N (N=N2, N3, N5, N6) bond lengths slightly stretch 0.007 Å, the axial Co1–N (N=N1, N4) bond lengths are contracted by 0.009 Å. The largest change in bond angles of **2** is a value of 0.35° observed in the N(2)–Co(1)–N(1) angle of $[Co(dien)_2]^{2+}$. The Sn–Se bond lengths in **2** are shortened somewhat. However, others angles change little (table S1 of the Supplementary material).

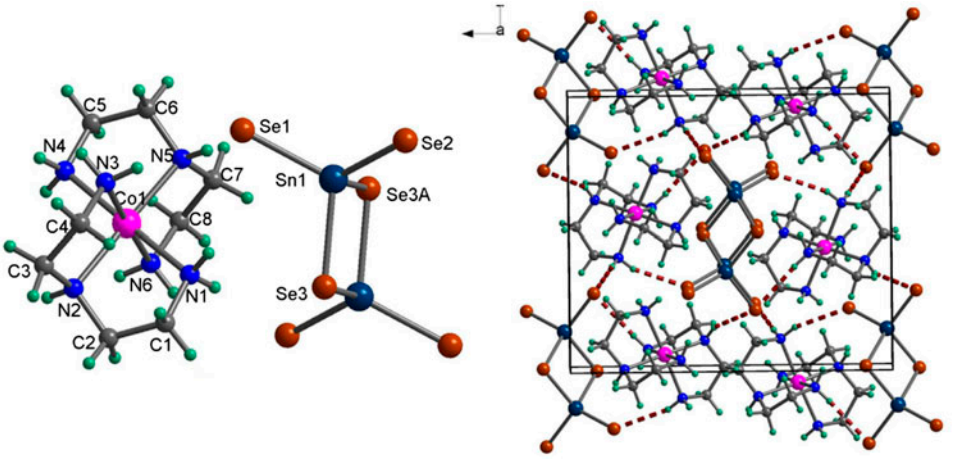

Figure 1. (a) Perspective view of $[Sn_2Se_6]^{4-}$ and $[Co(dien)_2]^{2+}$ in **1**. (b) Perspective view of the 3-D supramolecular array of **1**.

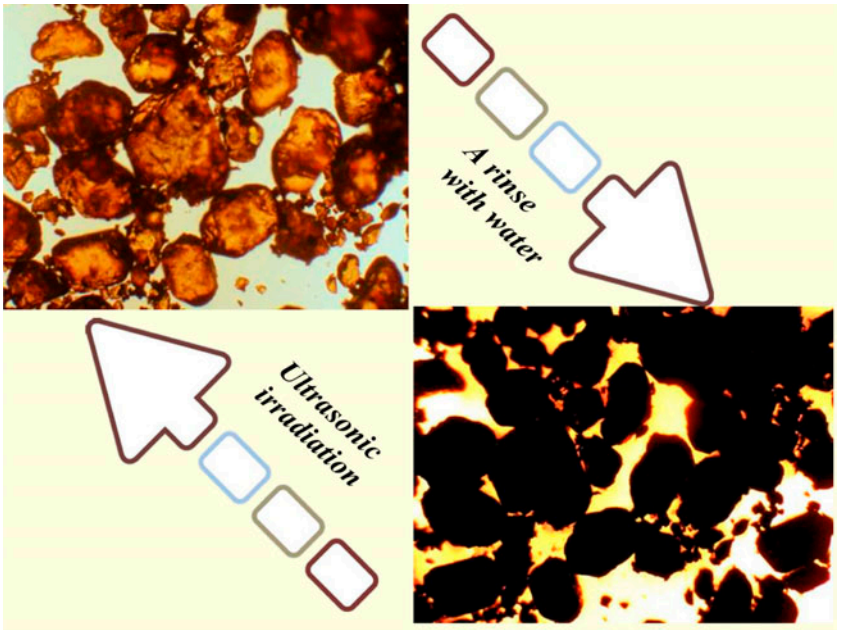

Figure 2. Ultrasonic–chromic properties of the title complex.

3.2. *Chromism*

Compound **1** shows interesting chromic transformation from yellow crystals to black **2** by a rinse with water, and the chromic reversal can be accomplished upon ultrasonic irradiation (figure 2). Compound **1** is sensitive to water and turns into black **2** after rinsing for several hours (figure 2). However, the color change does not occur when rinse is carried out in alcohol, which indicates that chromism of **1** is significantly solvent-dependent. In order to check genuine chromism or just a surface phenomenon, black **2** was cut into pieces, which

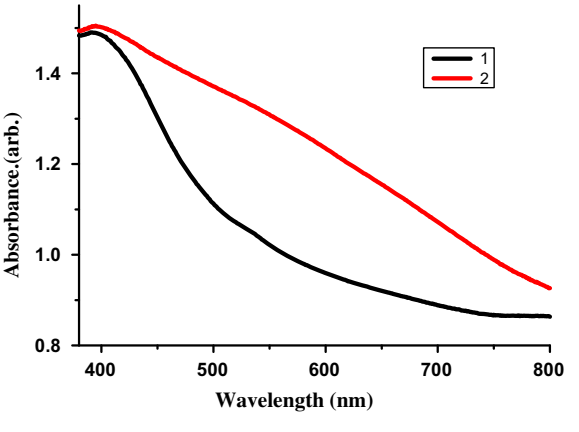

Figure 3. Absorption spectra of **1** (black line) and **2** (red line) (see http://dx.doi.org/10.1080/00958972.2014.901505 for color version).

show not only the surface but also the core of the crystals are black (figure S3 of the Supplementary material). This demonstrates that the chromism of **1** is not a surface reaction but a genuine solvent chromism. In contrast to solvent chromism, black **2** is sensitive to ultrasonic radiation. Upon ultrasonic irradiation for several minutes, black **2** turns into yellow **1**. The frequency for the ultrasonic-induced transformation of **2** is 40 kHz, and a slightly higher frequency more readily causes color change. However, black **2** is stable in air for over two months.

Figure 3 shows the visible solid absorption spectra of **1** and **2**. Absorption intensities of **1** are much weaker, especially around the visible absorption band. Via a rinse with water, yellow **1** turned into black **2** and the corresponding absorption intensities around 550 nm increased. It is found around 550 nm as a flattened shoulder rather than a clear absorption band in the absorption spectrum (figure 3) [36]. The addition of the absorption intensities was regarded as a hyperchromism [37, 38], which can be considered to arise mainly from the van der Waals interaction between two excited chromophores in the 3-D supramolecular ordered structure.

3.3. *Luminescent properties*

Solid-state luminescent properties of **1** and **2** were investigated at ambient temperature (figure 4). After excitations at 358.5 and 366 nm, both display a similar blue emission with a maximum at 435 nm and a shoulder 418 nm (figure 4). The emission takes place with large Stokes shift compared with the absorption. Compared with **2**, **1** exhibits much larger emission intensity. As early as 1995, Blasse reported that luminescence is promoted by edge and face sharing of the polyhedra involved [39]. Probably sharing-edge SnSe tetrahedra in the anionic $[Sn_2Se_6]^{4-}$ also plays a dominating role in this charge transfer process. It is well known that compounds of d^{10} ions can show efficient luminescence due to charge-transfer transitions, but luminescence from higher valence ions with d^{10} configuration is seldom mentioned [40]. The spectral bands involved in the luminescence of **1** and **2** might be

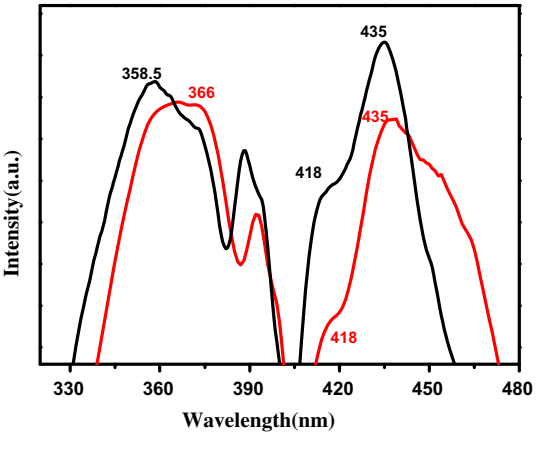

Figure 4. Emission and excitation spectra of **1** and **2**: excitation spectrum of **1** (λ_{max} = 358.5 nm) (black) and emission spectrum of **1** (λ_{max} = 435 nm) (black); excitation spectrum of **2** (λ_{max} = 366 nm) (red) and emission spectrum of **2** (λ_{max} = 440 nm) (red) (see http://dx.doi.org/10.1080/00958972.2014.901505 for color version).

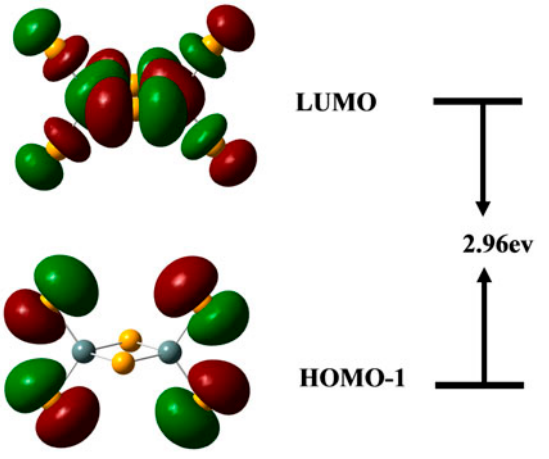

Figure 5. Electron density distribution and orbital gap of the HOMO-1; LUMO frontier orbitals calculated for $[Sn_2Se_6]^{4-}$.

assigned to charge-transfer transitions involving Sn(IV) and selenium in the anionic $[Sn_2Se_6]^{4-}$. However, the nature of this emission is not yet completely clear.

To understand the emission mechanism, time-dependent density functional theory calculations using the B3LYP functions have been performed on the model complex $[Sn_2Se_6]^{4-}$ with a ground-state geometry adapted from the X-ray data. The calculated results indicate that the main transitions are dominated by HOMO-1→LUMO transitions. As shown in figure 5, the electron density of the HOMO-1 is composed of 4p orbitals of Se, while the LUMO is dominated by 5s orbitals of Sn and 4p orbitals of Se atoms. Comparing with the electron density of the HOMO-1, electron density of the LUMO of 4p orbitals of Se decreased. On the basis of the above calculations, the emission band centered at 435 nm may be assigned to a Se–Sn charge transfer. Compared with the calculation gaps 2.96 eV (HOMO-1–LUMO for $[Sn_2Se_6]^{4-}$), the experimentally measured emission energy values are ca. 2.85 eV.

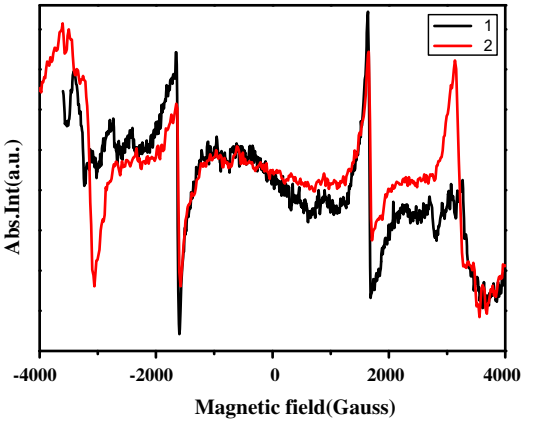

Figure 6. EPR spectrum of **1** (black line) and **2** (red line) at room temperature (see http://dx.doi.org/10.1080/00958972.2014.901505 for color version).

3.4. *EPR spectroscopy*

The room temperature EPR spectra for **1** and **2** are anisotropic. Compound **1** exhibited two EPR signals at $g = 4.22$ and $g = 2.19$ (figure 6). Generally, isoelectronic ions in similar symmetry environments have similar g factors, and metal ions with a $3d^7$ configuration, such as Fe(I), Co(II), and Cu(IV) [41]. Hence, the two EPR signals in **1** may be ascribed to the presence of Co(II) with $3d^7$ configuration. After rinsing, the EPR intensities of **2** decreased, but the intensity of signal centered at $g = 2.19$ sharply increases. This might be indicative of transformation from high spin ($S = 3/2$) to low spin ($S = 1/2$) state.

4. Conclusion

We have prepared a new chalcogenidostannate under hydrothermal conditions, which consists of $[Sn_2Se_6]^{4-}$ and an octahedral complex cation $[Co(dien)_2]^{2+}$. The title complex exhibited reversible chromism varying from yellow to black. By investigating the optical properties, it is possible that van der Waals interaction between two excited chromophore groups in the 3-D supramolecular structure with an ordered structure result in the chromism.

Supplementary material

Crystallographic data, characterization data, a Microsoft PowerPoint to show solvent induced reversible chromism of yellow **1** to black **2**, and a video to show ultrasound chromism of **2** to **1** have been deposited as a supplementary data.

Funding

This work was supported by National Basic Research Program of China [973 Program 2012CB821701]; IRT1156; National Science Fund for Distinguished Young Scholars [20925101].

References

[1] M. Russo, S.E.J. Rigby, W. Caseri, N. Stingelin. *Adv. Mater.*, **24**, 3015 (2012).
[2] M.S. Wang, G.C. Guo, W.Q. Zou, W.W. Zhou, Z.J. Zhang. *Angew. Chem. Int. Ed.*, **47**, 3565 (2008).
[3] P.C. Jhang, N.T. Chuang, S.L. Wang. *Angew. Chem. Int. Ed.*, **49**, 4200 (2010).
[4] C.J. Huber, T.C. Anglin, B.H. Jones, N. Muthu, C.J. Cramer, A.M. Massari. *J. Phys. Chem. A*, **116**, 9279 (2012).
[5] Z.Z. Yuan, C.W. Lee, S.H. Lee. *Angew. Chem. Int. Ed.*, **43**, 4197 (2004).
[6] J. Areephong, W.R. Browne, N. Katsonis, B.L. Feringa. *Chem. Commun.*, 3930 (2006).
[7] T. Tsukuda, M. Kawase, A. Dairiki, K. Matsumoto, T. Tsubomura. *Chem. Commun.*, **46**, 1905 (2010).
[8] E. Cariati, X.H. Bu, P.C. Ford. *Chem. Mater.*, **12**, 3385 (2000).
[9] K. Motoyama, H.F. Li, T. Koike, M. Hatakeyama, S. Yokojima, S. Nakamura, M. Akita. *Dalton Trans.*, 10643 (2011).
[10] W.Q. Mu, Q.Y. Zhu, L.S. You, X. Zhang, W. Luo, G.Q. Bian, J. Dai. *Inorg. Chem.*, **51**, 1330 (2012).
[11] C.T. Poon, W.H. Lam, V.W.W. Yam. *J. Am. Chem. Soc.*, **133**, 19622 (2011).
[12] K. Motoyama, T. Koike, M. Akita. *Chem. Commun.*, 5812 (2008).
[13] H.O. Stephan, M.G. Kanatzidis. *J. Am. Chem. Soc.*, **118**, 12226 (1996).
[14] G.M. Sheldrick. *SHELXTL-97 Program for Crystal Structure Solution and Refinement*, University of Göttingen, Germany (1997).
[15] D.X. Jia, J. Dai, Q.Y. Zhu, Y. Zhang, X.M. Gu. *Polyhedron*, **23**, 937 (2004).

[16] A. Fehlker, R. Blachnik. *Z. Anorg. Allg. Chem.*, **627**, 411 (2001).
[17] C.Y. Tang, F. Wang, W.Q. Jiang, Y. Zhang, D.X. Jia. *Inorg. Chem.*, **52**, 10860 (2013).
[18] W.W. Tang, C.Y. Tang, F. Wang, R.H. Chen, Y. Zhang, D.X. Jia. *J. Solid State Chem.*, **199**, 287 (2013).
[19] J. Zhao, J.J. Liang, Y.L. Pan, Y. Zhang, D.X. Jia. *Monatsh. Chem.*, **142**, 1203 (2011).
[20] J. Zhou, L.T. An, X. Liu, L.J. Huang, X.J. Huang. *Dalton Trans.*, 11419 (2011).
[21] W. Bensch, C. Näther, R. Stähler. *Chem. Commun.*, 477 (2001).
[22] R. Stähler, B.D. Mosel, H. Eckert, W. Bensch. *Angew. Chem. Int. Ed.*, **41**, 4487 (2002).
[23] R. Stähler, C. Näther, W. Bensch. *J. Solid State Chem.*, **174**, 264 (2003).
[24] R. Stähler, C. Näther, W. Bensch. *Eur. J. Inorg. Chem.*, 1835 (2001).
[25] R. Stähler, W. Bensch. *Z. Anorg. Allg. Chem.*, **628**, 1657 (2002).
[26] J.R. Li, Z.L. Xie, X.W. He, L.H. Li, X.Y. Huang. *Angew. Chem. Int. Ed.*, **50**, 11395 (2011).
[27] X. Chen, X.Y. Huang, A. Fu, J. Li, L.D. Zhang, H.Y. Guo. *Chem. Mater.*, **12**, 2385 (2000).
[28] S. Haddadpour, M. Melullis, H. Staesche, C.R. Mariappan, B. Roling, R. Clérac, S. Dehnen. *Inorg. Chem.*, **48**, 1689 (2009).
[29] P.W. Menezes, T.F. Fässler. *Z. Anorg. Allg. Chem.*, **638**, 1109 (2012).
[30] P.N. Trikalitis, K.K. Rangan, T. Bakas, M.G. Kanatzidis. *J. Am. Chem. Soc.*, **124**, 12255 (2002).
[31] P.N. Trikalitis, N. Ding, C. Malliakas, S.J.L. Billinge, M.G. Kanatzidis. *J. Am. Chem. Soc.*, **126**, 15326 (2004).
[32] D.X. Jia, A.M. Zhu, J. Deng, Y. Suzhou. *Z. Anorg. Allg. Chem.*, **633**, 1246 (2007).
[33] S. Dehnen, C. Zimmermann. *Z. Anorg. Allg. Chem.*, **628**, 2463 (2002).
[34] D.X. Jia, Q.X. Zhao, Y. Zhang, J. Dai, J. Zhou. *Eur. J. Inorg. Chem.*, 2760 (2006).
[35] D.X. Jia, Y. Zhang, Q.X. Zhao, J. Deng. *Inorg. Chem.*, **45**, 9812 (2006).
[36] H. Konaka, L.P. Wu, M. Munakata, T. Kuroda-Sowa, M. Maekawa, Y. Suenaga. *Inorg. Chem.*, **42**, 1928 (2003).
[37] C. Imbert, H.P. Hratchian, M. Lanznaster, M.J. Heeg, L.M. Hryhorczuk, B.R. McGarvey, H.B. Schlegel, C.N. Verani. *Inorg. Chem.*, **44**, 7414 (2005).
[38] Y.R. Kim, L. Gong, J. Park, Y.J. Jang, J. Kim, S.K. Kim. *J. Phys. Chem. B*, **116**, 2330 (2012).
[39] G. Blame, M.A. Hamrtra, D.J.W. IJdo, J.R. Plaisier. *Mater. Res. Bull.*, **30**, 967 (1995).
[40] G. Blasse, B.C. Grabmaier. *Luminescent Materials*, p. 53, Springer-Verlag, Berlin (1994).
[41] X.M. Zhang, J. Lv, F. Ji, H.S. Wu, H.J. Jiao, P.R. Schleyer. *J. Am. Chem. Soc.*, **133**, 4788 (2011).